

REVIEW ARTICLE

Spin-orbit coupling and electron spin resonance for interacting electrons in carbon nanotubes

A De Martino[†], R Egger[†] [§], F Murphy-Armando[‡] and K Hallberg[‡]

[†] Institut für Theoretische Physik, Heinrich-Heine-Universität, D-40225 Düsseldorf, Germany

[‡] Instituto Balseiro, Centro Atómico Bariloche, Comisión Nacional de Energía Atómica, 8400 S.C. de Bariloche, Argentina

Abstract. We review the theoretical description of spin-orbit scattering and electron spin resonance in carbon nanotubes. Particular emphasis is laid on the effects of electron-electron interactions. The spin-orbit coupling is derived, and the resulting ESR spectrum is analyzed both using the effective low-energy field theory and numerical studies of finite-size Hubbard chains and two-leg Hubbard ladders. For single-wall tubes, the field theoretical description predicts a double peak spectrum linked to the existence of spin-charge separation. The numerical analysis basically confirms this picture, but also predicts additional features in finite-size samples.

PACS numbers: 71.10.-w, 73.63.Fg, 76.30.-v

Submitted to: *J. Phys.: Condens. Matter*

[§] To whom correspondence should be addressed (egger@thphy.uni-duesseldorf.de)

1. Introduction

Nanotubes constitute a new class of mesoscopic quantum wires characterized by the interplay of strong electron-electron interactions, low dimensionality, disorder, and unconventional spin dynamics [1, 2, 3, 4, 5, 6, 7]. In a sense, they represent an ideal model for strongly correlated mesoscopic systems, where in fact basically all known effects in mesoscopic physics have been experimentally observed. Two main classes of nanotubes can be distinguished, namely single-wall nanotubes (SWNTs) which consist of just one wrapped-up graphene sheet, and multiwall nanotubes which contain additional inner shells [5]. Here we will focus on the conceptually simpler SWNTs, where interactions completely destroy the standard Fermi liquid picture and lead to a so-called Luttinger liquid (LL) state of matter [6]. Evidence for the LL behaviour of interacting 1D electrons has been reported for charge transport in SWNTs [2, 3, 4]. However, in such materials one also expects to find more dramatic consequences of the breakdown of Fermi liquid theory, most notably the phenomenon of spin-charge separation. This many-body effect asserts that electrons brought into a LL effectively break up into a charge and a spin part that travel with different velocities and hence will be spatially separated after some time. A recent proposal to detect spin-charge separation in SWNTs has been based on spin transport [7]. A different (and perhaps easier to realize) proposal based on electron spin resonance (ESR) is reviewed in this paper, expanding on our short paper [8]. ESR is a valuable experimental tool to probe the intrinsic spin dynamics of many systems. In ESR experiments one applies a static magnetic field and measures the absorption of radiation polarized perpendicular to the field direction. In the absence of $SU(2)$ spin symmetry breaking terms in the Hamiltonian, the absorption intensity is then simply a δ -peak at the Zeeman energy [9, 10].

Since spin-orbit (SO) interactions are generally the leading terms breaking the $SU(2)$ invariance, deviations in the ESR intensity from the δ -peak, e.g. shifts or broadenings, are directly connected to these couplings. Below we theoretically address the spin-orbit interaction and the resulting ESR spectrum for interacting SWNTs, using both a continuum field theory and a Hubbard model description. Within the effective field theory, the single δ -peak is split into two narrow peaks in SWNTs if spin-charge separation is realized. Otherwise the ESR spectrum would form a broad band with thresholds at the lower and upper edge [11]. This qualitative difference is caused by the fact that the SO interaction in SWNTs does not spoil spin-charge separation to leading order. Experimental observation of the peak splitting could therefore provide strong evidence for the elusive phenomenon of spin-charge separation [12]. To experimentally check the predictions made below, samples free of magnetic impurities have to be used. Such impurities have probably spoiled previous ESR measurements for nanotubes [5].

The outline of this article is as follows. In Section 2 the Luttinger liquid theory is briefly reviewed, and we also give a short introduction to ESR theory relevant for our purposes. The spin-orbit interaction is derived in detail in Section 3, followed by a discussion of the low-energy theory prediction for the ESR spectrum in Section 4.

An alternative approach is to use numerical methods to compute the ESR spectrum for microscopic lattice fermion models. We shall use both a Hubbard chain and the more realistic two-leg Hubbard ladder formulation of interacting SWNTs [13]. While charge transport does not allow for such a description due to the importance of long-range interactions, it turns out that for ESR spectra, only short-range interactions are important. These are correctly captured by Hubbard-type models, and therefore such models are expected to be appropriate for the quantitative description of ESR spectra in SWNTs. We discuss this approach in Section 5 and compare the numerical results with the field-theoretical predictions. Finally, in Section 6 conclusions and a brief outlook are provided. In most of the paper, we use the conventions $\hbar = c = 1$ to simplify notation.

2. Basics

2.1. Luttinger liquid theory

The Luttinger liquid is the low-energy description of metallic 1D (single-channel) quantum wires [12]. In SWNTs, due to the presence of two distinct gapless K points in the first Brillouin zone, there are actually two “flavours” corresponding to excitations close to these two points [1]. In addition, the spin degree of freedom is of particular interest to us, and to keep the $SU(2)$ spin symmetry at all stages, we shall not use the Abelian bosonization but rather employ the Sugawara formulation [12] which manifestly respects $SU(2)$ spin invariance. This formulation is in fact fully equivalent to a Wess-Zumino-Witten theory, even with the additional flavour degeneracy [12]. Since our main interest is on spin properties, we shall however suppress the flavour index for now, but return to the complexities added by it later, see Section 5. It is then sufficient to use the standard charge ($J_{L/R}$) and spin currents $\vec{J}_{R/L}$ for right (R) and left (L) moving electrons described by chiral 1D fermion operators $\psi_{R/L}(x, t)$. In terms of these field operators, chiral $SU(2)$ spin current operators are given by

$$\vec{J}_{R,L}(x) = \frac{1}{2} : \psi_{R/L}^\dagger(x) \vec{\sigma} \psi_{R/L}(x) :, \quad (1)$$

where the colons denote normal-ordering and Pauli matrices $\vec{\sigma}$ act in spin space. They obey Kac-Moody commutation relations ($\mu, \nu = x, y, z$)

$$[J_{L/R}^\mu(x), J_{L/R}^\nu(x')] = \pm i\delta'(x - x')\delta^{\mu\nu}/4\pi + i\epsilon^{\mu\nu\lambda} J_{L/R}^\lambda(x)\delta(x - x'). \quad (2)$$

Likewise, charge current operators are defined as

$$J_{R,L} =: \psi_{R/L}^\dagger(x) \psi_{R/L}(x) :, \quad (3)$$

where spin indices are summed over.

The Luttinger liquid Hamiltonian H_0 for a metallic system of interacting 1D spin-1/2 electrons is conventionally described using Abelian bosonization [12], with charge/spin interaction parameters $K_c < 1, K_s$, and charge/spin velocities $v_{c/s} = v_F/K_{c/s}$. In nanotubes, the Fermi velocity is $v_F = 8 \times 10^5$ m/sec, and $SU(2)$ invariance is usually implemented by fixing $K_s = 1$ [12]. Inclusion of magnetic Zeeman fields

B (orbital effects play no role here) only affects the spin sector and in general could renormalize K_s . However, this renormalization is irrelevant to ESR, which probes the finite energy scale $\approx B$ [9].

Here we shall proceed along a slightly different path using the $U(1) \times SU(2)$ invariant Sugawara formulation [12],

$$H_0 = H_c + H_s, \quad (4)$$

with decoupled charge and spin parts. The charge sector is described by the $U(1)$ invariant Hamiltonian

$$H_c = \frac{\pi v_c}{2} \int dx (: J_R J_R + J_L J_L : + g_c : J_L J_R :). \quad (5)$$

The coupling g_c and the charge velocity v_c are determined by the Fermi velocity v_F and the Luttinger parameter K_c . For explicit expressions, see [12]. In the noninteracting limit, $g_c = 0$ and $v_c = v_F$. The $SU(2)$ invariant spin Hamiltonian H_s commuting with H_c is

$$H_s = \frac{2\pi v_s}{3} \int dx : \vec{J}_R \cdot \vec{J}_R + \vec{J}_L \cdot \vec{J}_L : + g_s \int dx : \vec{J}_R \cdot \vec{J}_L :, \quad (6)$$

where v_s is the spin velocity (which is of the order v_F), and g_s is the coupling constant for electron-electron backscattering processes. We note in passing that $g_s \propto 1/R$ with the SWNT radius R , and hence this coupling causes only exponentially small gaps [6]. However, in a dynamical spin-sensitive ESR measurement, such thermodynamic reasoning might not be valid [7]. The LL Hamiltonian (4) completely decouples when expressed in terms of spin and charge currents (or the spin/charge bosons of Abelian bosonization). This remarkable fact leads to the phenomenon of spin-charge separation, and unless the spin-orbit interaction couples spin and charge sectors, ESR will only probe the spin sector.

Finally, we mention recent experimental observations of LL behaviour in SWNTs [2, 3, 4], where charge transport power laws were consistently explained within this framework. Probing spin properties of individual SWNTs has however so far remained a largely open issue.

2.2. Electron spin resonance

Adopting the standard Faraday configuration, the ESR intensity at frequency ω is proportional to the Fourier transform of the transverse spin-spin correlation function [9],

$$I(\omega) = \int dt e^{i\omega t} \langle S^+(t) S^-(0) \rangle, \quad (7)$$

where the static magnetic field points along the z -axis, $\vec{S} = \sum_i \vec{S}_i$ is the total spin operator, and $S^\pm = S^x \pm iS^y$. The Hamiltonian can be written as $H = H_0 + H_Z + H'$, where H_0 represents the $SU(2)$ invariant nanotube model (4) including electron-electron interactions, $H_Z = -g_e \mu_B \vec{B} \cdot \vec{S}$ is the Zeeman term (below, often $g_e \mu_B = 1$), and H' represents $SU(2)$ spin-symmetry breaking terms, in particular the SO coupling.

Inserting a complete set of eigenstates $|a\rangle$ of H in equation (7), the ESR intensity follows as

$$I(\omega) = \frac{1}{Z} \sum_{a,b} e^{-E_b/k_B T} \delta(\omega - (E_a - E_b)) |\langle a | S^- | b \rangle|^2. \quad (8)$$

In the absence of H' , there are only contributions from matrix elements between eigenstates with equal total spin $S_a = S_b$. Then all states with $S_a^z = S_b^z - 1$ will lead to a δ -peak at frequency $\omega = B$. For instance, at zero temperature, the application of a magnetic field B , taken as large enough to overcome a spin gap possibly present at $B = 0$, leads to a ground state with finite magnetization, $S_0 \neq 0$, and the states with $S_a^z = S_0^z - 1$ again yield the δ -peak. This can be made explicit as follows. Since $[H_0 + H_Z, S^-] = BS^-$, one has $(H_0 + H_Z)S^-|0\rangle = S^-(H_0 + H_Z)|0\rangle + BS^-|0\rangle$ and identifying $S^-|0\rangle = |a\rangle$, one gets $E_a = E_0 + B$ and thus $I(\omega) = I_0\delta(\omega - B)$. Any perturbation preserving $SU(2)$ invariance will neither shift nor broaden this peak, even at finite temperature [10]. To get nontrivial ESR spectra, one has to identify the leading perturbation breaking $SU(2)$ invariance, which will cause finite linewidth and shift of the ESR peak. In metallic systems like SWNTs, one has to consider the spin-orbit (SO) interaction. This is done in the next section.

3. Spin-Orbit Coupling

In our derivation of the SO term, we shall neglect electron-electron interactions. Local electric fields exerted by other electrons on a given electron are typically weak compared to the ionic fields [14], and will generally only weakly renormalize the SO couplings from their noninteracting values. In a single-particle picture, the SO interaction then appears because an electron moving in the electrostatic potential $\Phi(\vec{r})$ experiences an effective magnetic field $\vec{v} \times \nabla\Phi$ in its rest frame. With $\vec{p} = m\vec{v}$ the SO interaction reads in second-quantized form

$$H' = -\frac{g_e \mu_B}{4m} \int d\vec{r} \Psi^\dagger [(\vec{p} \times \nabla\Phi) \cdot \vec{\sigma}] \Psi. \quad (9)$$

The electron spinor field $\Psi_\sigma(\vec{r})$ living on the tube surface, $\vec{r} = (x, y)$ with \hat{e}_x parallel to the tube axis and y pointing around the circumference, can be expressed in terms of the electron operators c_i for honeycomb lattice site i at \vec{r}_i ,

$$\Psi_\sigma(\vec{r}) = \sum_i \chi(\vec{r} - \vec{r}_i) c_{i\sigma}, \quad (10)$$

where $\chi(\vec{r} - \vec{r}_i)$ is the corresponding Wannier wavefunction centered at lattice site \vec{r}_i . These localized Wannier orbitals can be chosen as real-valued functions even when hybridization with s -orbitals is important. For the simplest case, $2p_z$ orbital wavefunctions could be used, with z perpendicular to the graphene plane,

$$\chi(\vec{r}) = (z/4a_0\sqrt{2\pi}) \exp(-r/2a_0),$$

where $a_0 = \hbar^2/6me^2$ is the effective Bohr radius.

Inserting the expansion (10) into (9), the SO interaction reads [8, 15, 16],

$$H' = \sum_{\langle jk \rangle} i c_j^\dagger (\vec{u}_{jk} \cdot \vec{\sigma}) c_k + \text{H.c.} \quad (11)$$

which explicitly breaks $SU(2)$ symmetry. The SO vector $\vec{u}_{jk} = -\vec{u}_{kj}$ has real-valued entries and can be written as

$$\vec{u}_{jk} = \frac{g_e \mu_B}{4m} \int d\vec{r} \Phi(\vec{r}) [\nabla \chi(\vec{r} - \vec{r}_j) \times \nabla \chi(\vec{r} - \vec{r}_k)]. \quad (12)$$

The on-site term ($j = k$) is identically zero, and since the overlap decreases exponentially with $|\vec{r}_j - \vec{r}_k|$, we keep only nearest-neighbour terms in equation (11). Equation (11) also allows to incorporate electric fields due to impurities or close-by gate electrodes. To connect the SO vector to the experimentally measurable SO relaxation rate, τ_{SO}^{-1} , we estimate this rate using Fermi's golden rule. Assuming a constant \vec{u} , the probability for a transition from the initial state $|i\rangle = |k, \uparrow\rangle$ to the final state $|f\rangle = |k', \downarrow\rangle$ is given by $\Gamma_{i \rightarrow f} = 2\pi |\langle f | H' | i \rangle|^2 \delta(E_i - E_f)$, and summing over all final states,

$$\tau_{SO}^{-1} = 8(u_x^2 + u_y^2)/3v_s. \quad (13)$$

For SWNTs, SO couplings are generally expected to be small. This is in accordance with our approach since the SO vector (12) vanishes by symmetry for an ideal 2D honeycomb lattice. A finite nearest-neighbour SO coupling can only arise due to the finite curvature, stray fields from nearby gates, or due to impurities, which break the high symmetry. Focusing for clarity on the curvature-induced SO coupling, the SO vector for achiral tubes can be seen to only depend on bond direction,

$$\vec{u}_{\vec{r}_i, \vec{r}_i + \vec{\delta}_a} = \vec{u}_a, \quad (14)$$

where the nearest-neighbour bonds $\vec{\delta}_a$ ($a = 1, 2, 3$) connect the two sublattices of the graphene sheet in real space. For explicit representations of the vectors $\vec{\delta}_a$, see e.g. [16]. From now on we then restrict our analysis to achiral tubes.

4. ESR spectrum from field theory

Starting from a microscopic lattice description of the SWNT, inclusion of the interactions among electrons leads to rather complicated models. In the case of short-ranged interactions, one can study Hubbard-type models, and we will do so in Section 5. A different approach is to restrict attention to low energy scales compared to the scale $D = \hbar v_F / R$, which is of the order 1 eV in typical SWNTs, and construct a continuum field theory [6]. In this theory, the lattice electron field operators (10) are converted into slowly varying 1D fermions by expanding in Bloch states and keeping only the transverse momenta for which energy bands intersect the Fermi surface. Other transverse momenta are then separated by energies of the order D , and can safely be omitted in the regime of validity of the theory.

Applying this program to the SO interaction (11) is straightforward and leads to the following picture. The continuum version of the SO coupling, up to terms that are

irrelevant in the renormalization group sense, can be written as $H' = H_1 + H_2$, with the relevant perturbation (scaling dimension one)

$$H_1 = \int dx \vec{\lambda} \cdot (\vec{J}_L - \vec{J}_R), \quad (15)$$

and the marginal perturbation (scaling dimension 2)

$$H_2 = \int dx \sum_{r=R/L} \psi_r^\dagger \vec{\lambda}' \cdot \vec{\sigma} i \partial_x \psi_r + \text{H.c.} \quad (16)$$

With the unit vector \hat{e}_x along the tube axis, we find effective SO vectors given in terms of the vectors specified in (14),

$$\vec{\lambda} = 2 \text{ Im} \sum_a e^{i\vec{K} \cdot \vec{\delta}_a} \vec{u}_a, \quad \vec{\lambda}' = \sum_a e^{i\vec{K} \cdot \vec{\delta}_a} (\hat{e}_x \cdot \vec{\delta}_a) \vec{u}_a, \quad (17)$$

where \vec{K} denotes the coordinates of the K point in the first Brillouin zone. In our derivation, following standard reasoning, we have neglected oscillatory terms that average out on large length scales. These oscillations are governed by the wavevector $2|\mu|/v_F$ corresponding to the doping level μ . For a commensurate situation (undoped case), however, additional terms do arise that are ignored in this section. In the following, we will keep only the leading contribution (15) and neglect the marginal term H_2 . In the numerical analysis of Section 5, the full SO interaction will be considered to assess the accuracy of these approximations. Since SO couplings are typically very small, however, the above perturbative reasoning, suggesting to drop H_2 and the oscillatory terms, is expected to work.

Remarkably, the SO interaction then acts exclusively in the spin sector and hence does not spoil spin-charge separation. Therefore the ESR intensity can be computed from the spin sector alone. For convenience, we define

$$\vec{\lambda}_{r=R/L=\pm} = \vec{B} \pm \vec{\lambda}, \quad (18)$$

which represents an effective magnetic field acting separately on the chiral (right/left-moving) spin currents. The presence of two pseudo-fields already hints at the outcome of our calculation below, namely the emergence of a double peak spectrum. Their position will then be given by the absolute values $\lambda_r = |\vec{\lambda}_r|$. The spin Hamiltonian governing the ESR spectrum $I(\omega)$ is then with H_s in (6) and the Zeeman term given by

$$H = H_s - \sum_r \int dx \vec{\lambda}_r \cdot \vec{J}_r. \quad (19)$$

The Heisenberg equation of motion for the chiral spin current operators is

$$(\partial_t \pm v_s/3\partial_x) \vec{J}_r = \mp (g_s/4\pi) \partial_x \vec{J}_{-r} + g_s \vec{J}_R \times \vec{J}_L - \vec{\lambda}_r \times \vec{J}_r. \quad (20)$$

Taking $\vec{B} = B \hat{e}_z$, and using $\vec{S} = \vec{J}_R + \vec{J}_L$, the ESR spectral density is

$$I(\omega) = \int dt dx e^{i\omega t} \sum_{rr'} \langle J_r^+(x, t) J_{r'}^-(0, 0) \rangle. \quad (21)$$

We then compute the ESR spectrum using the Sugawara spin Hamiltonian (19). An independent route would proceed via fermionization [8]. For simplicity, we discuss the

case $g_s = 0$ (no backscattering), but the method is flexible enough to allow treatment of the general case as well. However, the numerical analysis of Section 5 indicates that indeed the backscattering interaction does not affect the results in a significant way.

Since the spin Hamiltonian decouples in the chiral spin currents, we just need to add the contributions due to the two chiralities. In equilibrium, using the spin susceptibility $1/4\pi v_s$ of a chiral fermion, we have

$$\langle \vec{J}_R \rangle = \frac{1}{4\pi v_s} \vec{\lambda}_R. \quad (22)$$

Using the fluctuation-dissipation theorem, we can now express $I(\omega)$ in (21) in terms of the imaginary part of the susceptibility tensor $\chi_r(q, \omega)$,

$$I(\omega) = \sum_{r=\pm} \sum_{\mu, \nu=x, y} \frac{2}{1 - \exp(-\omega/k_B T)} \text{Im} \chi_r^{\mu\nu}(q \rightarrow 0, \omega). \quad (23)$$

The susceptibility can in turn directly be obtained from the equation of motion (20). Formally defining the matrix $(\Lambda_r)^{\mu\nu} = \epsilon^{\mu\nu\alpha} \lambda_r^\alpha$, we find

$$\chi_r(q \rightarrow 0, \omega) = \frac{1}{4\pi v_s} [i\omega + \Lambda_r]^{-1} \Lambda_r,$$

and straightforward algebra then yields the ESR spectrum

$$I(\omega) = \sum_{r=\pm} [1 + \lambda_r^z / \lambda_r]^2 \frac{\lambda_r}{4v_s(1 - e^{-\lambda_r/k_B T})} \delta(\omega - \lambda_r). \quad (24)$$

As expected, the single δ -peak splits into two peaks but there is no broadening. The peak separation is $|\lambda_+ - \lambda_-|$, see (18), and the peak heights are generally different. To lowest order in λ/B , the two peaks are located symmetrically around $\omega = B$. Notice that for \vec{B} perpendicular to the effective SO vector $\vec{\lambda}$, the splitting is zero.

It should be stressed that these results hold both for the non-interacting and the interacting case. However, for the interacting case realized in SWNTs the double peak structure is only possible if spin-charge separation is present. Otherwise the charge sector will mix in, leading to broad bands with threshold behaviours [11]. Closer inspection shows that inclusion of the subleading term (16) preserves the splitting into two peaks, but the peaks now acquire a finite width $\sim |\vec{\lambda}'|$. Similarly, the effects of backscattering are expected to be small. Experimental observation of the predicted double-peak spectrum could then provide strong evidence for spin-charge separation. In practice, to get measurable intensities, one will have to work with an ensemble of SWNTs. The proposed experiment may be possible using electric-field-aligned SWNTs, or by employing arrays of identical SWNTs. In more conventional samples with many SWNTs, however, the SO vector $\vec{\lambda}$ can take a random direction. For results on the averaged spectrum, see [8].

5. ESR spectra for armchair SWNTs: Two-leg Hubbard ladders

In this section we discuss an alternative description of the ESR spectrum via a lattice fermion description. We shall numerically compute ESR spectra for a Hubbard chain

and a two-leg Hubbard ladder [13]. These models ignore the long-range part of the Coulomb interactions which makes them less accurate for the description of charge transport. Since the long-range tails of the interaction do not affect the spin dynamics, however, this does not create a problem for the spin problem at hand.

Modelling the SWNT by a two-leg Hubbard ladder is attractive for the following reasons:

- Backscattering interactions as well as commensurability effects (Umklapp scattering) are included.
- The two flavour degrees of freedom are taken care of.
- Band curvature effects are taken into account.
- The marginal SO term (16) as well as all irrelevant contributions can be kept.
- For the Hubbard chain, it is known that any magnetic field spoils spin-charge separation [17]. The importance of this effect for SWNTs can be assessed.
- Accurate numerical techniques are available for such models.

To gain a broader perspective and to also make contact to other 1D conductors, before dealing with the more complex two-leg ladder system, we first consider a 1D Hubbard chain [12] with uniform SO coupling,

5.1. Hubbard chain

The 1D Hubbard model with a uniform SO coupling vector $\vec{\lambda}$ is defined by

$$H = \sum_n \left[c_n^\dagger (-t + i\vec{\lambda} \cdot \vec{\sigma}) c_{n+1} + \text{H.c.} \right] + U \sum_n n_{n\uparrow} n_{n\downarrow} - B \sum_n S_n^z. \quad (25)$$

For $\vec{\lambda} = 0$, equation (25) leads to a LL phase at low energies [12]. It is worth noting that then the exact solution of (25) shows that with a magnetic field, the charge and spin sectors get mixed [17]. To make progress, we gauge away the SO term by the unitary transformation

$$c_n \rightarrow d_n = \begin{cases} c_n & (n \text{ odd}), \\ \exp(i\alpha \hat{\lambda} \cdot \vec{\sigma}) c_n & (n \text{ even}), \end{cases}$$

where $\alpha = \arctan(\lambda/t)$, $\hat{\lambda} = \vec{\lambda}/\lambda$ with $\lambda = |\vec{\lambda}|$. The hopping amplitude then changes as $t \rightarrow \tilde{t} = t + \lambda \sin \alpha$, and one can easily see that $n_{n\uparrow} n_{n\downarrow} = \tilde{n}_{n\uparrow} \tilde{n}_{n\downarrow}$, where $\tilde{n}_{n\sigma} = d_{n\sigma}^\dagger d_{n\sigma}$. Then the Hamiltonian (25) can be rewritten as

$$H = -\tilde{t} \sum_n (d_n^\dagger d_{n+1} + \text{H.c.}) + U \sum_n \tilde{n}_{n\uparrow} \tilde{n}_{n\downarrow} - B \sum_n \tilde{S}_n^z,$$

and the spin operator as

$$\tilde{S}_n = \begin{cases} \frac{1}{2} d_n^\dagger \vec{\sigma} d_n & (n \text{ odd}), \\ \frac{1}{2} d_n^\dagger (e^{i\alpha \hat{\lambda} \cdot \vec{\sigma}} \vec{\sigma} e^{-i\alpha \hat{\lambda} \cdot \vec{\sigma}}) d_n & (n \text{ even}). \end{cases}$$

The transformed picture is easier to use in practical calculations. We have calculated the ESR spectrum for (25) using exact diagonalization for small lattices.

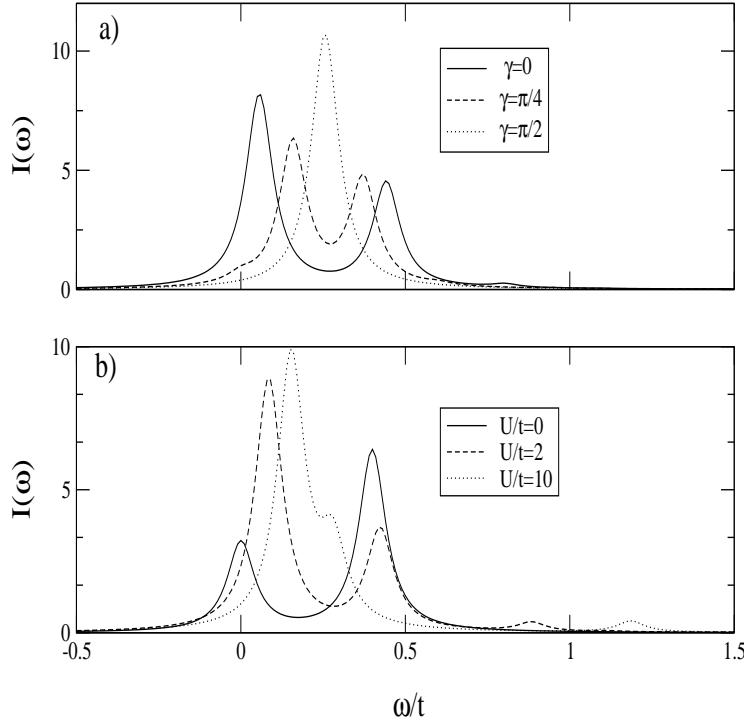


Figure 1. Exact diagonalization results for the $T = 0$ ESR spectra of a Hubbard chain with $\lambda = 0.1$, $B/t = 0.2$, and artificial broadening $0.05t$. In (a) ESR spectra for $U/t = 1$ are shown for different angles γ between $\vec{\lambda}$ and \vec{B} . In (b) the U -dependence is shown for $\gamma = 0$. All results are for 12 lattice sites and 4 electrons.

The main features emerging from exact diagonalization can be seen in figure 1. For weak interactions, see figure 1(a), we recover the two-peak structure predicted by field theory, see (24), with the peaks symmetrically arranged around $\omega = B$ but with different peak heights. In addition, no splitting is seen for \vec{B} perpendicular to the SO vector $\vec{\lambda}$. The interaction dependence of the ESR spectrum is shown in figure 1(b). Strong interactions suppress one of the peaks and enhance the other, and also give rise to more structure in the spectrum. This behaviour can be traced back to the effects of band curvature. Note that for increasing U , the distance between both peaks decreases. This feature can be qualitatively explained by a decrease of the spin velocity v_s with U , *i.e.* for a flatter band, the spin-orbit splitting is less effective.

5.2. Two-leg Hubbard ladder: Armchair SWNTs

We are now ready to generalize the above treatment to armchair SWNTs. Mapping the interacting honeycomb lattice Hamiltonian for armchair SWNTs onto the two-leg Hubbard model [13], one finds

$$H_0 = \sum_{ni} (-tc_{ni}^\dagger c_{(n+1)i} - t_\perp c_{n1}^\dagger c_{n2} + \text{H.c.}) + U \sum_{n,i} n_{n,i,\uparrow} n_{n,i,\downarrow}. \quad (26)$$

While under the mapping, $t_\perp = t$ up to $1/R$ corrections [13], we shall allow for $t_\perp \neq t$ to have better numerical accuracy. Here we also want to include the spin-orbit interaction (11) in this mapping. We use the SO vectors (14), and for simplicity set $\vec{u}_1 = 0$, since this SO vector does not appear in the leading low-energy SO vector $\vec{\lambda}$ in (17) for armchair SWNTs. This simplification also allows for numerically feasible calculations. Writing $\vec{w}_n = (-1)^n \vec{W} + \vec{w}$, where $\vec{w} = (\vec{u}_2 - \vec{u}_3)/2$ and $\vec{W} = (\vec{u}_2 + \vec{u}_3)/2$, the spin-orbit term can then be written as

$$H' = \sum_n i(c_{n,1}^\dagger \vec{w}_n \cdot \vec{\sigma} c_{n+1,1} + c_{n,2}^\dagger \vec{w}_{n+1} \cdot \vec{\sigma} c_{n+1,2}) + \text{H.c.}, \quad (27)$$

consisting of a uniform and an alternating contribution,

$$c_{n,1/2}^\dagger \vec{w}_n \cdot \vec{\sigma} c_{n+1,1/2} = c_{n,1/2}^\dagger \vec{w} \cdot \vec{\sigma} c_{n+1,1/2} \pm (-1)^n c_{n,1/2}^\dagger \vec{W} \cdot \vec{\sigma} c_{n+1,1/2}.$$

The resulting model is studied in the remainder of this section for the special case that both \vec{w} and \vec{W} are parallel to the uniform magnetic field. Note that \vec{w} corresponds to the leading SO vector $\vec{\lambda}$ in the low-energy theory, while \vec{W} is related to the subleading vector $\vec{\lambda}'$, see equation (17). Moreover, away from half-filling, following standard reasoning, one may expect that the alternating terms average out. Nevertheless, they will be kept below, but we indeed confirm that in large systems they lead only to small effects. When the above gauge transformation is applied again, we arrive at a two-leg Hubbard ladder (26), but with the on-chain hoppings t carrying both a uniform phase $\exp(i\phi_u)$ and an alternating phase $\exp(i\phi_a)$ determined by \vec{w} and \vec{W} , respectively, see figure 2.

Let us first discuss the noninteracting case. For $U = 0$, the solution of equations (26) and (27) is straightforward. The eigenenergies are given by (a is the lattice constant)

$$E_{1\pm}(k_x) = -\sqrt{(2t \cos(k_x a + \sigma\phi_u))^2 \pm 4tt_\perp \cos(k_x a + \sigma\phi_u) \cos(\phi_a) + t_\perp^2}$$

$$E_{2\pm}(k_x) = \sqrt{(2t \cos(k_x a + \phi_u))^2 \pm 4tt_\perp \cos(k_x a + \phi_u) \cos(\phi_a) + t_\perp^2}$$

where $\sigma = \pm 1$ for up or down electrons respectively. In figure 3 we show the non-interacting $T = 0$ ESR spectrum in the presence of both the uniform and the alternating phase. The main excitations contributing to each peak are sketched in figure 3(b). The uniform phase case (see dotted line) produces a splitting of the principal Zeeman peak. Due to the different parity of the $k = 0$ and $k = \pi$ bands, for the pure uniform case there is no ESR interband transition. When the alternating phase is turned on, the folding of the Brillouin zone produces peaks at higher energies. As the parity symmetry is broken, interband transitions are now possible. The opening of the small gap due to the alternating phase is manifested in the splitting seen in peaks A, B and C. The

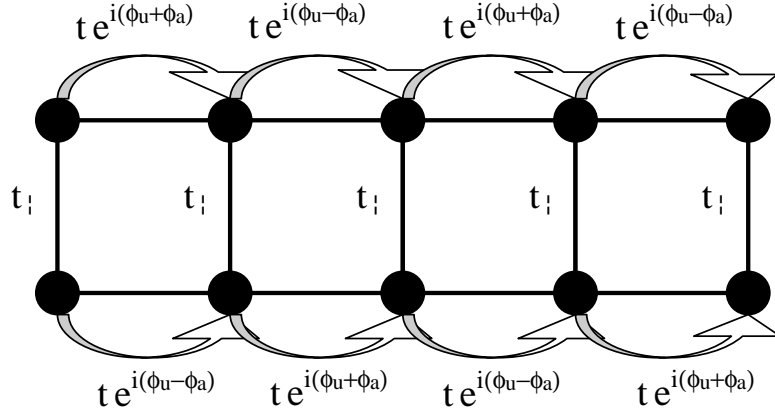


Figure 2. Sketch of the two-leg Hubbard ladder including spin-orbit couplings of the type considered here. The arrows indicate the phase for spins up. Spins down have the opposite phase.

broad structure (F and D) between the highest peaks correspond to transitions between branches with opposite curvature.

Next we discuss results for $U > 0$ using the density matrix renormalization group (DMRG) technique [18, 19]. We have used periodic boundary conditions keeping 256 states and the finite-system algorithm. The ESR spectrum (7) at $T = 0$ has been calculated using the dynamical DMRG technique [20, 21] for a two-leg ladder with uniform phase ϕ_u only. Additional small alternating phases ϕ_a did not change the spectrum significantly. In figure 4 we present these results for a quarter filled chain and $t_{\perp} = 1.2$ and $t = 1$. These parameters are used in order to clearly see the effect of the SO coupling, since for this filling the excitations occur near the linear term of the cosine bands for system sizes that are multiple of 4. The effect of the correlations mainly consists of a small shift of the peaks, but the double peak spectrum is preserved. Therefore the numerical results lend support to the basic prediction of the analytical low-energy theory, and show that the expected double-peak ESR spectrum is stable with respect to the above-mentioned perturbations.

6. Conclusions

We have reviewed the analysis of the ESR spectrum produced by the spin-orbit coupling in SWNTs. The effective field theory analysis shows that at low energy the SO interaction only acts in the spin sector and the single Zeeman peak, characteristic of a system with $SU(2)$ spin symmetry, is splitted into two peaks with no broadening. This result relies in an essential way on the property of spin-charge separation characteristic of the Luttinger liquid state realized in the SWNT. Thus the observation of such a splitting would directly point to this so far elusive feature.

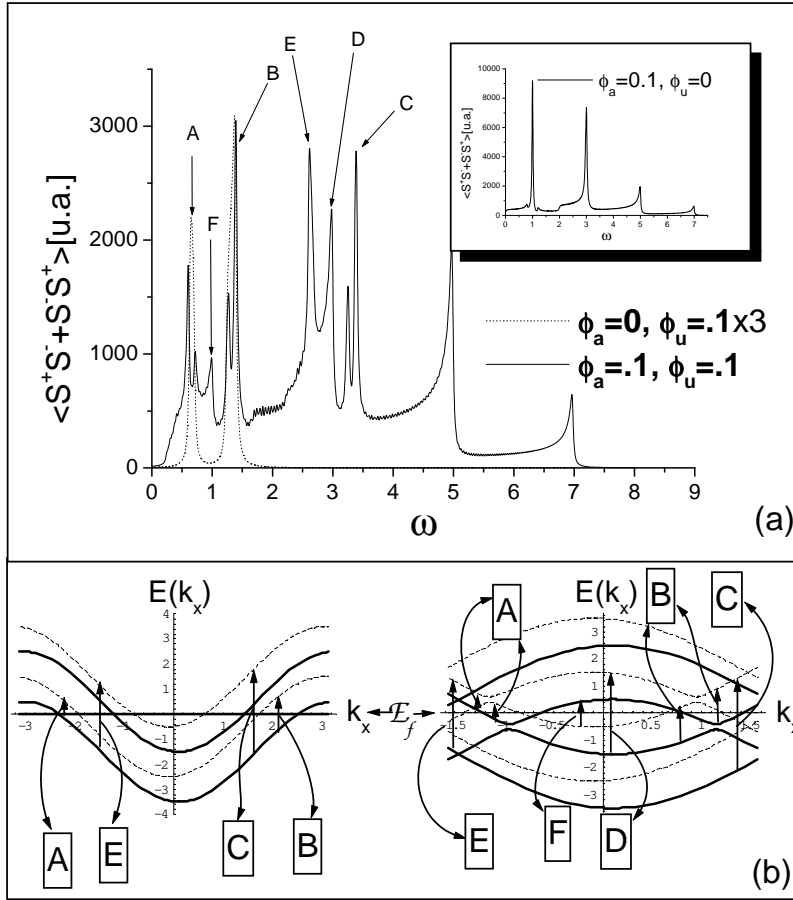


Figure 3. a) ESR spectrum and b) dispersion relation of the non-interacting model for $t = t_\perp = 1$ and different phase configurations. The dotted (full) lines in (b) correspond to spins down (up).

The field theory analysis has been complemented by the exact numerical calculation of the ESR spectrum for Hubbard models on a single chain and on a two-leg ladder. While these models are not able to describe reliably the charge transport properties of SWNTs due to neglect of the long-range tails of the Coulomb interaction, they are appropriate descriptions of the spin problem at hand. The numerical analysis confirms the field theory results, assessing also the validity of the approximations involved in their derivation. In addition, it reveals additional structure in the spectrum due to band curvature and higher energy processes, which are not captured by the field theory approach.

Acknowledgments

We thank C.A. Balseiro for the collaboration in the first stage of this work and L. Forró for valuable discussions. Support by the DFG under the Gerhard-Hess program, and by

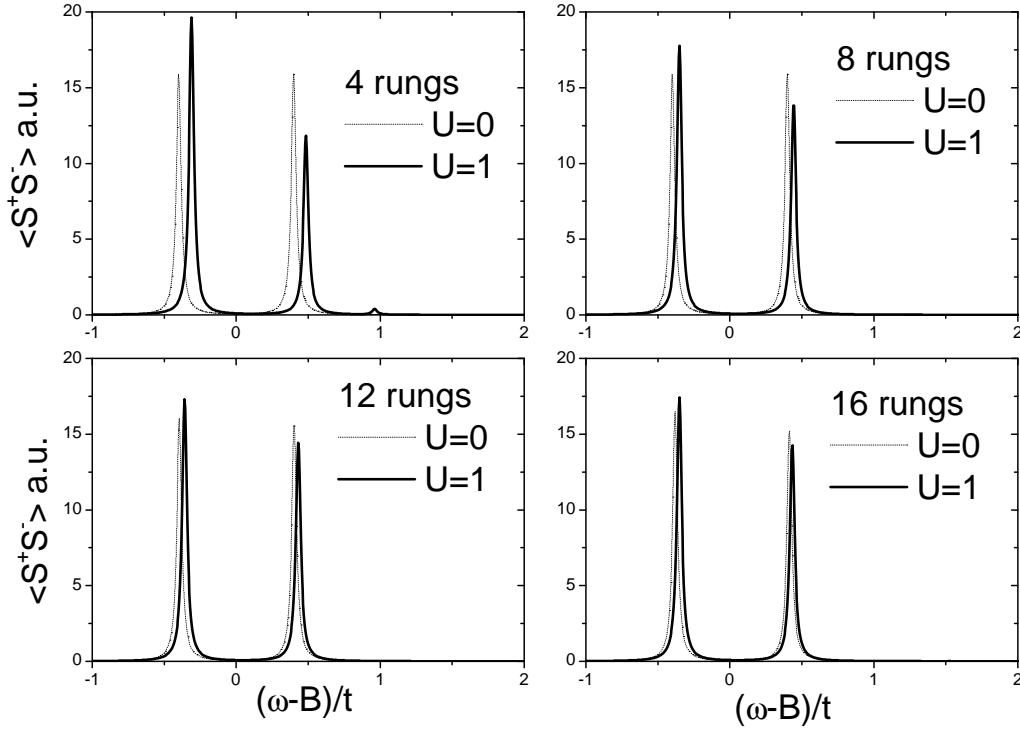


Figure 4. ESR spectra for periodic quarter-filled ladders with a uniform phase $\phi_u = 0.1$, $t = 1$ and $t_{\perp} = 1.2$.

the project PICT 99 3-6343 is acknowledged.

References

- [1] Dekker C 1999 *Physics Today* **52**(5) 22
- [2] Bockrath M, Cobden D H, Lu J, Rinzler A G, Smalley R E, Balents L and McEuen P L 1999 *Nature* **397** 598
- [3] Yao Z, Postma H W C, Balents L and Dekker C 1999 *Nature* **402** 273
- [4] Postma H W C, Teepen T, Yao Z, Grifoni M and Dekker C 2001 *Science* **293** 76
- [5] Forró L and Schönenberger C 2001 *Topics in Appl. Phys.* **80** 1
- [6] Egger R and Gogolin A O 1997 *Phys. Rev. Lett.* **79** 5082; Kane C, Balents L and Fisher M P A 1997 *Phys. Rev. Lett.* **79** 5086
- [7] Balents L and Egger R 2001 *Phys. Rev. B* **64** 035310
- [8] De Martino A, Egger R, Hallberg K and Balseiro C A 2002 *Phys. Rev. Lett.* **88** 206402
- [9] Oshikawa M and Affleck I 1999 *Phys. Rev. Lett.* **82** 5136
- [10] Oshikawa M and Affleck I 2002 *Phys. Rev. B* **65** 134410
- [11] De Martino A and Egger R 2001 *Europhys. Lett.* **56** 570
- [12] Gogolin A O, Nersesyan A A and Tsvelik A M 1998 *Bosonization and Strongly Correlated Electron Systems* (Cambridge University Press)
- [13] Balents L and Fisher M P A 1997 *Phys. Rev. B* **55** 11973
- [14] Chen G H and Raikh M E 1999 *Phys. Rev. B* **60** 4826
- [15] Bonesteel N E 1993 *Phys. Rev. B* **47** 11302

- [16] Ando T 2000 *J. Phys. Soc. Jpn.* **69** 1757
- [17] Frahm H and Korepin V E 1990 *Phys. Rev. B* **42** 10553
- [18] White S 1992 *Phys. Rev. Lett.* **69** 2863; 1993 *Phys. Rev. B* **48**
- [19] Peschel I, Wang X, Kaulke M and Hallberg K 1998 *Density Matrix Renormalization* (Springer)
- [20] Hallberg K 1995 *Phys. Rev. B* **52** 9827
- [21] Murphy-Armando F 2002 *MSc Thesis* (Instituto Balseiro, Bariloche, Argentina)